Peroxisomal Biogenesis Disorder: Comparison of Conventional MR Imaging with Diffusion-Weighted and Diffusion-Tensor Imaging Findings

Birgitta S. M. ter Rahe, Charles B. L. M. Majoie, Erik M. Akkerman, Gerard J. den Heeten, Bwee T. Poll-The, and Peter G. Barth

BACKGROUND AND PURPOSE: **Peroxisomal biogenesis disorders (PBDs) refer to a group of disorders of peroxisomal biogenesis causing neuronal migration disorder, delayed myelination, and demyelination. The aim of this study was to evaluate the added value of diffusion-weighted imaging (DWI) and diffusion tensor imaging (DTI) compared with that of conventional T2-weighted imaging in assessing the extent of white matter damage in patients with PBDs.**

METHODS: **Three patients (aged 12, 16, and 80 months) with PBD (type 1 protein targeting sequence [PTS1]) and three age-matched control subjects underwent MR imaging on a 1.5-T system. The protocol included axial T2-weighted, DWI, and DTI sequences. Fractional anisotropy (FA) and apparent diffusion coefficient (ADC) changes were calculated using regions of interest at several predefined white matter areas and compared with those of age-matched control subjects. Color-coded maps were obtained to visualize the range of FA values.**

RESULTS: **On the T2-weighted images, one patient revealed severe hypomyelination throughout the brain; the two other patients showed focal abnormal high-signal-intensity areas. All patients had significantly decreased FA values in white matter areas that appeared abnormal on the T2-weighted images. In two of the three patients, significant FA reduction was also found in normal-appearing white matter. The ADC values of the patients were significantly increased compared with those of the age-matched controls.**

CONCLUSION: **Although based on a small number of patients, our data suggest that DWI and DTI can be used to characterize and quantify white matter tract injury in patients with PBD-PTS1. Furthermore, our data suggest that these techniques have the potential to identify neurodegenerative changes not yet visible on T2-weighted images.**

The peroxisome is a cellular organelle that participates in important cellular functions such as beta-oxidation of very-long-chain fatty acids (VLCFA) and plasmalogen production (1, 2). The abnormal fatty acids in peroxisomal disorders, particularly VLCFA and long-branched chain fatty acids (foremost phytanic acids), are incorporated into cell membranes and perturb their microenvironments, resulting in dysfunction, atrophy, and death of the cells. Impaired synthesis of plasmologens causes insufficiency and destruction of myelin (3).

Peroxisomal disorders are subdivided into two major categories (3). The first category includes the disorders of peroxisomal biogenesis or assembly, also called peroxisomal biogenesis disorder (PBD). PBD is characterized by abnormalities in neuronal migration or differentiation, defects in the formation or maintenance of central white matter, and postdevelopmental neuronal degenerations (3, 4). In these disorders, the peroxisome in the human cell is not formed normally, and several peroxisomal functions are deficient. The second category includes at least 10 disorders in which the defect involves a single peroxisomal protein and peroxisomal structure is intact (3).

PBD consists of a spectrum of diseases. Of them,

Received June 23, 2003; accepted after revision November 18.

Presented in part at the 18th Symposium Neuroradiologicum, Paris, August 2002, and the International Society for Magnetic Resonance in Medicine Workshop on MR of Childhood White Matter Disorders, Rotterdam, September 2002.

Supported by the Prinses Beatrix Fonds (grant MAR 98–0202).

From the Departments of Radiology (B.S.M.t.R., C.B.L.M.M., E.M.A., G.J.H.) and Pediatric Neurology (B.T.P.-T., P.G.B.), Academic Medical Center, Amsterdam, the Netherlands.

Address correspondence to Birgitta S. M. ter Rahe, MD, Department of Radiology, Academic Medical Center, P.O. Box 22660, 1100 DD Amsterdam, the Netherlands.

Zellweger syndrome (ZS) has the worst and infantile Refsum disease (IRD) the best prognosis. The pathophysiologic substrate of PBD is the impaired import of proteins into peroxisomes by a deviant peroxisomal membrane receptor for the peroxisome targeting sequence (PTS) (3). Proteins labeled with a PTS can pass the membrane of the peroxisome to the matrix. Impaired peroxisomal import of proteins by using the type 1 protein targeting sequence (PTS1) leads to biochemical impairments involving beta-oxidation of VLCFA, plasmalogen biosynthesis, and bile acid synthesis (1, 5). Impaired import of PTS1-labeled proteins causes ZS, neonatal adrenoleukodystrophy (NALD), and IRD. Impaired import of PTS2-labeled proteins causes rhizomelic chondrodysplasia punctata (3).

As demonstrated in previous studies, diffusion-weighted (DWI) and diffusion tensor imaging (DTI) are valuable methods for the evaluation of white matter tract integrity (6–14). They have the potential to detect neurodegenerative changes before conventional MR findings are abnormal (7).

In this study, we evaluated the added value of DWI and DTI in three children with PBD-PTS1 by comparing findings with those of conventional T2-weighted imaging, paying particular attention to the visualization of white matter lesions and quantification of their extent.

Methods

Three patients with PBD-PTS1 were referred for MR imaging. They included a 12-month-old boy with nutrition problems and a generalized hypotonia, epileptic seizures in terminal stage, and no motor and cognitive development; a 16-month-old girl who had nutrition problems, infantile spasms, and minimal head control at 1 year of age; and an 80-month-old girl who had no epileptic seizures and a normal motor development, but did present with nystagmus, cognitive delay, and no speech at 7 years of age. All three patients showed dysmorphism and had retinopathy, deafness, liver enlargement, and liver dysfunction. The final diagnosis PBD-PTS1 was proved with a liver biopsy in all three patients. They all had increased VLCFA in the plasma and a peroxin (PEX) gene 1. The first two patients had also decreased plasmalogens in erythrocytes. The children's ages were corrected for prematurity.

To take into account the age-related changes of cerebral white matter, we included three age-matched controls who were referred for MR imaging because of moderate nonprogressive mental retardation with unknown cause, degenerative and metabolic origin excluded. All of them had a normal degree of myelination and no pathologic changes.

Whole-brain MR investigations were performed on a 1.5-T system (Magnetom Vision; Siemens, Erlangen, Germany) by using a quadrature head coil. The imaging protocol included a para-axial fast spin-echo T2-weighted sequence with a TR/TE_{eff} of 3500/90 ms, an echo train length of 10, a field of view of 23 × 23 cm, an imaging matrix of 256 × 256, and a 5-mm section thickness with a 1.5-mm gap. DWI images were acquired with the same section thickness, gap, orientation, and section positions as those of the T2-weighted sequence and a field of view of 26 × 26 cm. A spin-echo echo-planar imaging sequence, a diffusion-sensitizing acquisition scheme, and a diffusion-sensitizing gradient pointing in six noncollinear directions was used as a means to gather complete diffusion tensor data (15). On the basis of the acquired data, the average apparent diffusion coefficient (ADC) and the fractional anisotropy (FA) were calculated (15). Color-coded FA maps were generated to visualize the range of FA values.

The images were loaded into Scion Image for Windows (Scion Corporation, Frederick, MD). Regions of interest of at least 12 pixels were placed by hand in predefined anatomic areas. In every region of interest, the mean and SD of the ADC and FA values were determined. In one patient, we repeated the procedure of placing and measuring regions of interest to get an indication of the reproducibility of the results.

Results

The T2-weighted images showed the following results. Images of the 12-month-old boy revealed diffuse hypomyelination and cortical dysplasia along the border of the right sylvian fissure. Those of the 16-month-old girl showed slight myelination delay in the parietal and deep frontal white matter bilaterally and in the white matter laterally of the bilateral cerebellar dentate nuclei. The bilateral internal capsules, the corona radiata bilaterally, and the genu and splenium of the corpus callosum appeared normal for her age. Images of the 80-month-old girl revealed normal myelination, but focal white matter lesions with high signal intensity in the splenium of the corpus callosum and the corona radiata and centrum semiovale were seen bilaterally.

The FA results for 12 predefined anatomic areas are summarized in the color maps of Figures 1 and 2 and in Table 1. As can be seen from the Figures and Table, FA was significantly decreased in the lesions visualized on the T2-weighted images. For all patients, FA values were significantly decreased in the parietal corona radiata and centrum semiovale bilaterally and the genu of the corpus callosum. The reproducibility of the FA measurements was good: there was 6% or less difference between the repeated measurements. FA was significantly decreased as well (compared with age-matched control subjects) in certain white matter areas that appeared normal on T2-weighted images in two of the three patients. In the 16-month-old girl, the most significant areas of FA decrease in normal-appearing white matter (NAWM) on T2-weighted images were: the parietal corona radiata bilaterally, the right frontal corona radiata, the anterior limbs of the bilateral internal capsules, the genu and splenium of the corpus callosum, the bilateral optic radiations, the white matter lateral of the bilateral cerebellar dentate nuclei, and the left cerebellar peduncle. In the 80-month-old girl, these areas were the genu and posterior limb of the internal capsules bilaterally, the anterior limb of the right internal capsule, the genu of the corpus callosum, the left optic radiation, and the bilateral cerebellar peduncles and cerebral peduncles.

The ADC could be reliably measured only for the centrum semiovale, frontal and parietal white matter, and the corpus callosum. The ADC values of abnormal-appearing white matter were significantly increased in the patients compared with those in age-matched control subjects (Table 2). For all three patients, the ADC values of the corona radiata and centrum semiovale

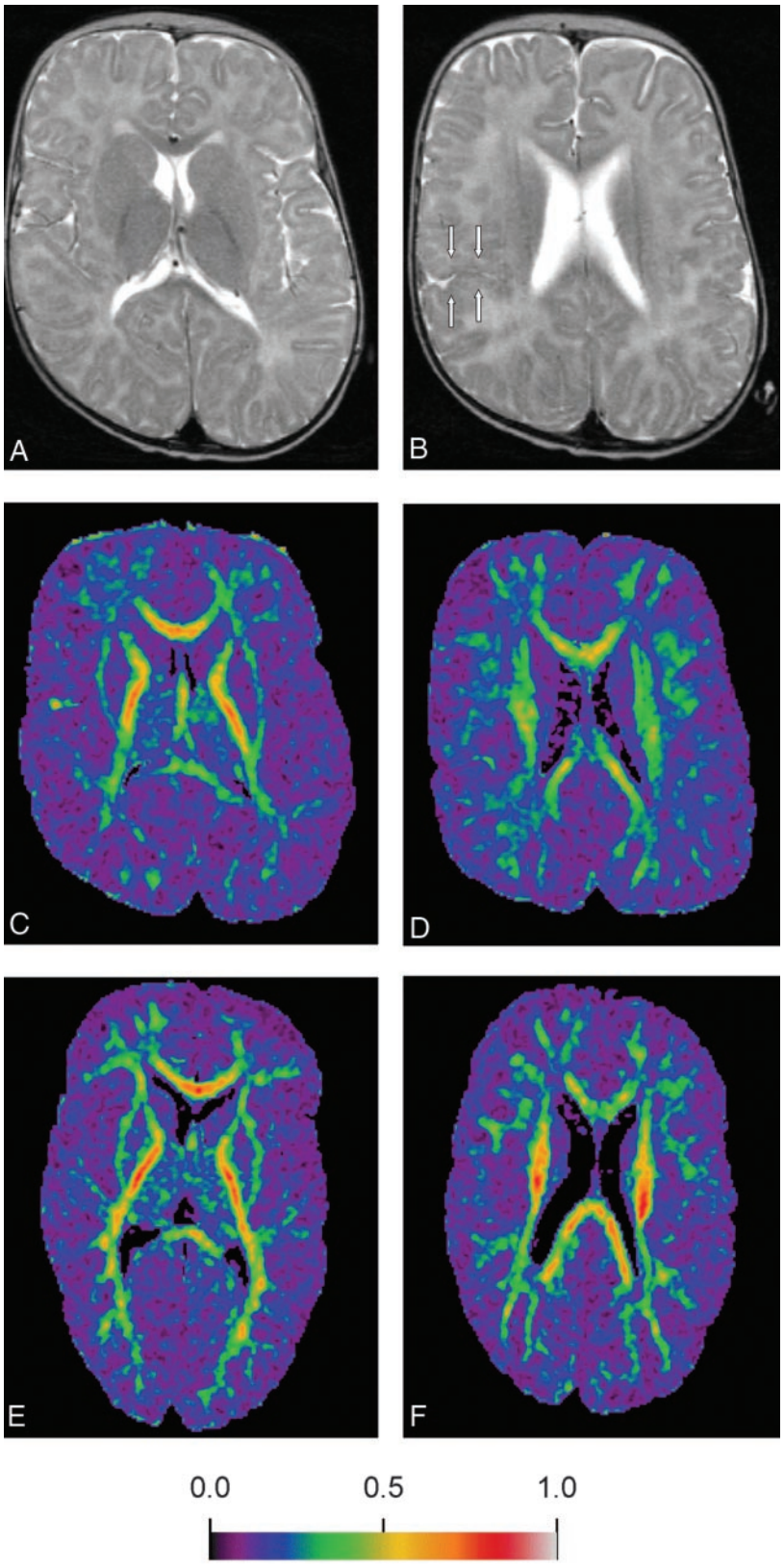

FIG 1. MR images obtained in a 12-month-old boy with biopsy-proved PBD-PTS1 (*A–D*) and in an age-matched girl with mental retardation (*E* and *F*).

A and *B,* Axial fast spin-echo T2-weighted images (3500/90/1 [TR/TE/NEX]) obtained in a 12-month-old boy, showing diffuse signal intensity increase in the white matter on the level of the anterior limb and genu of the internal capsules and the corona radiata bilaterally, which is consistent with hypomyelination. Posterior limbs of the bilateral internal capsules show hypomyelination. Cortical dysplasia along the border of the right sylvian fissure is present, as can be seen in PBDs (*arrows*).

C and *D,* Color-coded FA maps, demonstrating decreased anisotropy in the white matter at the same levels in this patient as those in the control subject (*E* and *F*).

E and *F,* Color-coded FA maps of the age-matched control subject of the corresponding levels as in panels *C* and *D*.

were significantly increased bilaterally compared with those of age-matched control subjects. ADC values were significantly increased in certain white matter areas that appeared normal on T2-weighted images in two of the three patients. In the 16-month-old girl, the most significant areas of ADC decrease in NAWM on T2-weighted images were the parietal and frontal corona radiata bilaterally and the genu and splenium of the corpus callosum. In the 80-month-old girl, this area was the genu of the corpus callosum.

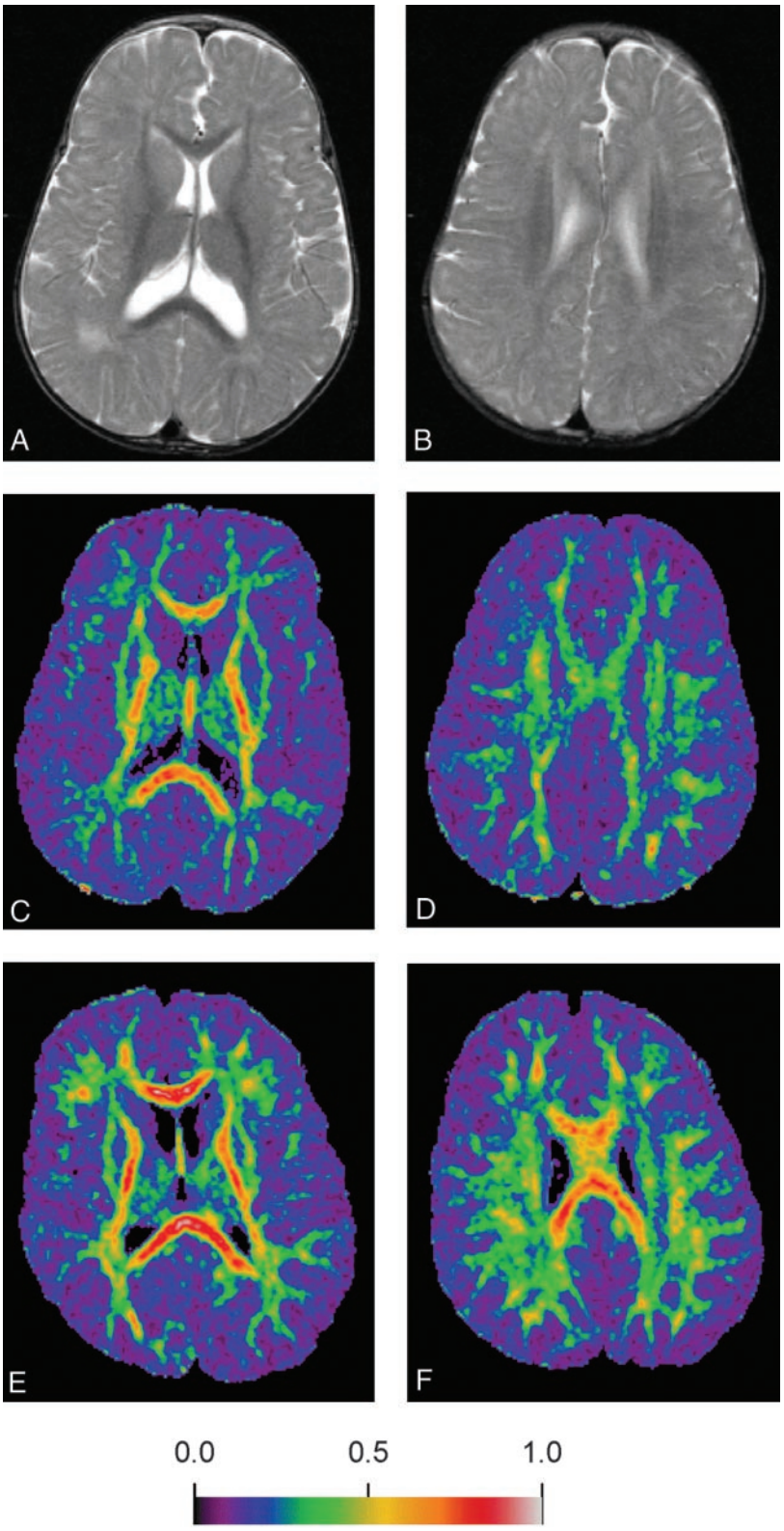

FIG 2. Images obtained in a 16-month-old girl with biopsy-proved PBD-PTS1 (*A–D*) and a control subject, an age-matched boy with mental retardation (*E* and *F*).

A and *B,* Axial fast spin-echo T2-weighted images (3500/90/1), showing high signal intensity in the parietal white matter bilaterally, but normal signal intensity in the bilateral internal capsules, the corpus callosum, and the corona radiata bilaterally.

C and *D,* Color-coded FA maps, demonstrating decreased anisotropy in the NAWM and abnormal-appearing white matter at the same levels as *A* and *B*, as compared with findings in the control subjects (*E* and *F).*

E and *F,* Color-coded FA maps of the age-matched control of the corresponding areas to *C* and *D.*

Discussion

All of the peroxisomal disorders with neurologic involvement may show abnormalities in white matter of the CNS and sometimes in the peripheral nerves. The extent of the abnormalities varies among the diseases. The hypothesis is that an abnormally high proportion of VLCFA is incorporated into membrane constituents perturbing membrane functions and into myelin leading to instability and spontaneous breakdown of myelin (dysmyelination) (3). Perhaps a direct cytotoxic effect on oligodendrocytes also occurs (3, 16). The incorporation of VLCFA into axonal mem-

TABLE 1: FA values in three patients with PBD and age-matched control subjects

		12 Months					16 Months					80 Months				
		Patient		Control			Patient		Control			Patient		Control		
FA values $\times 10^{-3}$		Mean (SD)	N	Mean (SD)	N	Diff.	Mean (SD)	N	Mean (SD)	N	Diff.	Mean (SD)	N	Mean (SD)	N	Diff.
White matter lateral to cerebellar	R	293 (45)	24	282 (36)	35	12	308 (46)	26	424 (47)	28	−116‡	471 (66)	40	559 (74)	73	−88‡
dentate nucleus	L	324 (43)	33	358 (68)	31	−34*	303 (43)	29	410 (72)	31	−107‡	461 (66)	57	490 (90)	56	−29*
Cerebellar peduncle	R	660 (46)	12	814 (48)	12	−153‡	753 (46)	12	788 (66)	12	−35	812 (59)	12	872 (42)	12	−60†
	L	751 (80)	12	882 (26)	12	−130‡	713 (67)	12	800 (48)	12	−86†	595 (39)	12	849 (70)	12	−254‡
Cerebral peduncle	R	526 (106)	39	677 (79)	15	−151‡	584 (96)	46	608 (128)	35	−24	515 (90)	37	722 (125)	76	−207‡
	L	591 (65)	26	585 (93)	34	6	608 (129)	37	642 (86)	34	−34	552 (77)	49	727 (84)	50	−175‡
Optic radiation	R	364 (35)	12	562 (32)	12	−198‡	507 (50)	12	599 (27)	12	−92‡	605 (32)	12	625 (51)	12	−20
	L	455 (45)	12	520 (58)	12	−65†	487 (27)	12	639 (74)	12	−152‡	505 (65)	12	740 (93)	12	−235‡
Genu of internal capsule	R	539 (32)	12	637 (79)	12	−98‡	611 (37)	12	604 (41)	12	7	544 (31)	12	777 (53)	12	−233‡
	L	561 (15)	12	582 (44)	12	−21	630 (39)	12	652 (69)	12	−22	658 (44)	12	809 (54)	12	−151‡
Posterior limb of internal capsule	R	564 (99)	83	666 (97)	66	−102‡	634 (144)	111	671 (117)	69	−37	613 (85)	124	734 (81)	79	−121‡
	L	572 (88)	92	657 (79)	58	−85‡	676 (101)	114	686 (75)	76	−10	663 (83)	107	747 (81)	98	−84‡
Anterior limb of internal capsule	R	493 (75)	48	511 (87)	30	−18	476 (95)	57	547 (85)	38	−71‡	487 (81)	42	676 (125)	39	−189‡
	L	508 (113)	48	575 (68)	18	−67*	508 (86)	62	599 (101)	33	−91‡	556 (114)	79	594 (107)	41	−38
Genu of corpus callosum		599 (72)	12	732 (60)	12	−133‡	544 (46)	12	908 (58)	12	−364‡	532 (88)	12	779 (101)	12	−247‡
Splenium of corpus callosum		532 (57)	12	523 (77)	12	9	695 (26)	12	893 (32)	12	−198‡	618 (57)	12	608 (104)	12	10
Parietal corona radiata	R	207 (33)	51	247 (75)	51	−40‡	237 (54)	51	301 (54)	51	−64‡	240 (41)	51	270 (89)	51	−30*
	L	162 (54)	51	199 (77)	51	−37†	170 (41)	51	280 (57)	51	−110‡	245 (59)	51	379 (77)	51	−134‡
Frontal corona radiata	R	214 (31)	51	227 (54)	51	−13	232 (42)	51	327 (52)	51	−95‡	362 (97)	51	423 (79)	51	−61‡
	L	184 (71)	51	221 (78)	51	−37*	252 (64)	51	249 (84)	51	3	339 (101)	51	403 (120)	51	−64†
Centrum semiovale	R	317 (28)	51	427 (109)	51	−110‡	432 (80)	51	465 (62)	51	−33*	446 (150)	51	559 (76)	51	−113‡
	L	318 (27)	51	407 (77)	51	−89‡	388 (54)	51	526 (82)	51	−138‡	442 (158)	51	507 (76)	51	−65†

Note.—N indicates number of pixels per region of interest; significance determined with *t* test: * $P < .05$; † $P < .01$; ‡ $P < .001$.

TABLE 2: ADC values in three patients with PBD and age-matched controls

		12 Months					16 Months					80 Months				
		Patient		Control			Patient		Control			Patient		Control		
ADC values $\times 10^{-3}$ mm^2/s		N	Mean (SD)	Mean (SD)	Diff.	%	Mean (SD)	Mean (SD)	Diff.	%		Mean (SD)	Mean (SD)	Diff.	%	
Genu of corpus callosum		12	111 (7)	107 (9)	4	4	98 (8)	75 (9)	22	30‡		92 (10)	69 (5)	24	35‡	
Splenium of corpus callosum		12	115 (12)	122 (23)	−7	−6	98 (9)	83 (7)	15	18‡		110 (10)	88 (16)	22	25‡	
Parietal corona radiata	R	51	131 (7)	106 (8)	25	24‡	117 (5)	102 (8)	15	15‡		102 (7)	93 (15)	8	9‡	
	L	51	137 (5)	108 (6)	30	28‡	129 (7)	109 (4)	20	19‡		94 (8)	91 (6)	2	3*	
Frontal corona radiata	R	51	127 (4)	105 (6)	23	22‡	115 (6)	91 (5)	24	27‡		94 (5)	73 (5)	20	28‡	
	L	51	124 (5)	110 (11)	14	13‡	114 (5)	94 (4)	21	22‡		92 (5)	84 (5)	8	10‡	
Centrum semiovale	R	51	131 (6)	95 (3)	35	37‡	106 (5)	100 (5)	6	6‡		100 (9)	84 (6)	16	20‡	
	L	51	141 (4)	94 (5)	47	49‡	110 (4)	99 (5)	11	11‡		95 (5)	91 (9)	4	4†	

Note.—N indicates number of pixels per region of interest; significance determined with *t* test: * $P < .05$; † $P < .01$; ‡ $P < .001$.

branes may interfere with normal receptor-neurotrophic factor interactions, resulting in axonal atrophy and loss in adrenomyeloneuropathy (3). Their incorporation into growth cone and radial glia plasmalemmae might impair neuronal migrations in ZS and the other dysmorphogenetic types. In adrenoleukodystrophy (ALD), these lipids seem to initiate a cascade of inflammatory demyelination that appears to be cytokine and T-cell mediated (3, 16).

Articles describing conventional MR imaging findings in PBD-PTS1 are few (1, 2, 17). According to these reports, ZS is characterized by a periventricular heterotopia and diminished myelination, which results in areas of diffuse high signal intensity on T2-weighted images and low signal intensity in white matter on T1-weighted images (1, 2). Also, diffuse abnormal cortical gyral patterns consisting of regions of microgyria (primarily in frontal and perisylvian cortex) and regions with thickened pachygyric cortex (primarily perirolandic and occipital) are common (1, 2). Barkovich and Peck (1) described an association with germinolytic cysts. NALD shows usually heterotopia, pachygyria, polymicrogyria, and diffuse demyelination (2). IRD may have normal MR imaging findings (2). Three patients with PBD in another study had an unusually late-onset white matter disease (5). On conventional MR images, cerebral demyelination with relative sparing of subcortical fibers and pronounced central cerebellar demyelination was shown (5).

DTI is an MR imaging technique that can provide information on white matter tract integrity by sensitizing MR images to the random motion of water

molecules (diffusion) in tissues (9, 10). Structures such as myelin sheaths, axonal membranes, and microfilaments cause the water diffusion to be slower perpendicular to axons than parallel to them, thereby leading to a diffusion anisotropy, which can be measured by using this technique (9, 10, 18). The extent to which diffusion is impaired by microstructures is then reflected by the degree of asymmetry, called FA. FA depends on axonal integrity and direction, fiber diameter, ensheathment of axons by intact oligodendrocytes, myelination, and some other factors, including sodium channel integrity (9, 11, 12). There is evidence that FA is a good measure for the structural integrity of a neuronal tract (8, 13).

Data from the literature suggest that DWI and DTI are valuable techniques for the characterization of hyperintense lesions on T2-weighted images in patients with leukodystrophy (6, 8, 14, 19). Ono and Engelbrecht (8, 14) have suggested that these techniques will be clinically useful to differentiate dysmyelination from demyelination. Both myelination abnormalities demonstrate similar high-signal-intensity lesions of the white matter on T2-weighted images. In dysmyelinating disorders such as Pelizaeus Merzbacher disease, diffusional anisotropy was still demonstrated in the white matter tracts, whereas demyelinating disorders such as Alexander disease, Krabbe disease, X–linked adrenoleukodystrophy (X-linked ALD), and mitochondrial disease lost diffusional anisotropy because of breakdown of myelin and destruction of axons resulting in a loss of diffusion barriers (7, 8, 14, 19). In one patient with ZS, increased ADC values and decreased anisotropy were found (8). X-linked ALD, a disorder caused by a single peroxisomal enzyme deficiency, is characterized by rapid demyelination with an inflammatory component triggered by the presence of VLCFA (7). In previous studies, increased ADC and decreased FA values were found in patients with X-linked ALD (7, 8). The drop in the FA is likely due to a breakdown of myelin and destruction of axons and, thus, a loss of diffusion barriers (7, 8). The increase in ADC is explained by an increase in free water and injury of the structures that restrict water diffusion (7, 8, 14). These findings from the literature are consistent with the data of our study. All patients with PBD-PTS1, a demyelinating disease, showed increase in ADC values and decrease in FA in most regions of interest, despite the differences in phenotype. Increased ADC values in the white matter are likely also due to an increase in free water in the extracellular space and injury to structures that restrict diffusion. The FA decrease suggests damage to myelinated white matter tracts.

DWI and DTI have the potential to identify neurodegenerative changes before the clinical onset of disease or before conventional MR findings become abnormal (7, 8). Previous studies have described ADC increase and FA decrease in NAWM in patients with X-linked ALD (7, 8). We also found abnormal DWI and DTI results in two of our patients in areas with NAWM on T2-weighted images. Larger studies with serial MR imaging are warranted to confirm whether DWI and DTI indeed have a higher sensitivity in detecting childhood white matter diseases than that of T2-weighted imaging.

In conclusion, although based on a small number of patients, our data suggest that DWI and DTI can be used to characterize and quantify white matter tract injury in patients with PBD-PTS1. Furthermore, they suggest that these techniques have the potential to identify neurodegenerative changes not yet visible on T2-weighted images. Larger studies with serial MR imaging are needed to validate these conclusions.

References

1. Barkovich AJ, Peck WW. **MR of Zellweger syndrome.** *AJNR Am J Neuroradiol* 1997;18:1163–1670
2. Van der Knaap MS, Valk J. **The MR spectrum of peroxisomal disorders.** *Neuroradiology* 1991;33:30–37
3. Powers JM, Moser H. **Peroxisomal disorders: genotype, phenotype, major neuropathologic lesions, and pathogenesis.** *Brain Pathol* 1998;8:101–120
4. Evrard P, Caviness VS, Prats-Vinas J, Lyon G. **The mechanism of arrest of neuronal migration in the Zellweger malformation: a hypothesis based upon cytoarchitectonic analysis.** *Acta Neuropathol* 1978;41:109–117
5. Barth PG, Gootjes J, Bode H, et al. **Late onset white matter disease in peroxisomal biogenesis disorder.** *Neurology* 2001;57:1949–1955
6. Melhem ER, Mori S, Mukundan G, et al. **Diffusion tensor MR imaging of the brain and white matter tractography.** *AJR Am J Roentgenol* 2002;178:3–15
7. Ito R, Melhem ER, Mori S, et al. **Diffusion tensor brain MR imaging in X-linked cerebral adrenoleukodystrophy.** *Neurology* 2001;56:544–547
8. Engelbrecht V, Scherer A, Rassek M, et al. **Diffusion-weighted MR imaging in the brain in children: findings in the normal brain and in the brain with white matter diseases.** *Radiology* 2002;222:410–418
9. Basser PJ, Pierpaoli C. **Microstructural and physiological features of tissues elucidated by quantitative-diffusion-tensor MRI.** *J Magn Reson B* 1996;111:209–219
10. Pierpaoli C, Jezzard P, Basser PJ, et al. **Diffusion tensor MR imaging of the human brain.** *Radiology* 1996;201:637–648
11. Hüppi PS, Maier SE, Peled S, et al. **Microstructural development of human newborn cerebral white matter assessed in vivo by diffusion tensor magnetic resonance imaging.** *Pediatr Res* 1998;44:584–590
12. Prayer D, Barkovich AJ, Kirschner DA, et al. **Visualization of nonstructural changes in early white matter development on diffusion-weighted MR images: evidence supporting premyelination anisotropy.** *AJNR Am J Neuroradiol* 2001;22:1572–1576
13. Mukherjee P, Miller JH, Shimony JS, et al. **Normal brain maturation during childhood: developmental trends characterized with diffusion-tensor MR imaging.** *Radiology* 2001;221:349–358
14. Ono J, Harada K, Mano T, et al. **Differentation of dys- and demyelination using diffusional anisotropy.** *Pediatr Neurol* 1997;16:63–66
15. Akkerman EM. **Efficient measurement and calculation of MR diffusion anisotropy images using the platonic variance method.** *Magn Reson Med* 2003;49:599–604
16. Powers JM, Liu Y, Moser AB, Moser HW. **The inflammatory myelinopathy of adreno-leukodystrophy: cells, effector molecules, and pathogenic implications.** *J Neuropathol Exp Neurol* 1992;51:630–643
17. Cheon JE, Kim IO, Hwang YS, et al. **Leukodystrophy in children: a pictorial review of MR imaging features.** *Radiographics* 2002;22:461–476
18. Schaefer PW, Grant PE, Gonzalez RG. **Diffusion-weighted MR imaging of the brain.** *Radiology* 2000;217:331–345
19. Majoie CB, Akkerman EM, Blank C, et al. **Mitochondrial encephalomyopathy: comparison of conventional MR imaging with diffusion-weighted and diffusion tensor imaging: case report.** *AJNR Am J Neuroradiol* 2002;23:813–816